

---

# WARPD: World model Assisted Reactive Policy Diffusion

---

**Shashank Hegde**  
University of Southern California  
khegde@usc.edu

**Satyajeet Das**  
University of Southern California

**Gautam Salhotra**  
(Google) Intrinsic LLC

**Gaurav S. Sukhatme**  
University of Southern California

## Abstract

With the increasing availability of open-source robotic data, imitation learning has become a promising approach for both manipulation and locomotion. Diffusion models are now widely used to train large, generalized policies that predict controls or trajectories, leveraging their ability to model multimodal action distributions. However, this generality comes at the cost of larger model sizes and slower inference, an acute limitation for robotic tasks requiring high control frequencies. Moreover, Diffusion Policy (DP), a popular trajectory-generation approach, suffers from a trade-off between performance and action horizon: fewer diffusion queries lead to larger trajectory chunks, which in turn accumulate tracking errors. To overcome these challenges, we introduce WARPD (World model Assisted Reactive Policy Diffusion), a method that generates closed-loop policies (weights for neural policies) directly, instead of open-loop trajectories. By learning behavioral distributions in parameter space rather than trajectory space, WARPD offers two major advantages: (1) extended action horizons with robustness to perturbations, while maintaining high task performance, and (2) significantly reduced inference costs. Empirically, WARPD outperforms DP in long-horizon and perturbed environments, and achieves multitask performance on par with DP while requiring only  $\sim 1/45th$  of the inference-time FLOPs per step.

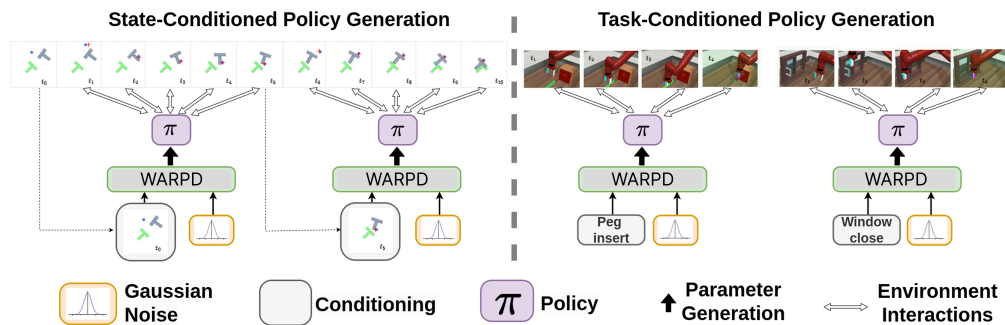


Figure 1: **WARPD** generates policies from heterogeneous trajectory data. With state-conditioned policy generation, the diffusion model can run inference at a lower frequency. With task-conditioned policy generation, the generated policies can be small yet maintain task-specific performance. Demonstrations of this work can be found on the project website: <https://sites.google.com/view/warpd/home>.

## 1 Introduction

The rise of open-source robotic datasets has made imitation learning a promising approach for robotic manipulation and locomotion tasks [11, 46]. While methods like Behavioral Cloning [14] and

transformer-based models (e.g., RT-1 [6]) have shown promise, they struggle with multimodal action distributions. For example, in navigation tasks where both “turn left” and “turn right” are valid, these models often predict an averaged action, i.e., “go straight”, leading to suboptimal performance.

Diffusion models offer a compelling alternative, providing continuous outputs and learning multimodal action distributions [54]. Action trajectory diffusion for robotic tasks [10] has shown promise but incurs high computational costs, particularly at high control frequencies. Moreover, such trajectory diffusion models are susceptible to the trade-off between performance and action horizon (or action chunk size, representing the number of environment interactions between consecutive trajectory generations). Fewer diffusion queries lead to larger action chunks, giving greater trajectory tracking errors.

To overcome these limitations, we introduce **World model Assisted Reactive Policy Diffusion (WARPD)**, a novel approach that uses latent diffusion and a world model to **generate closed-loop policies directly in parameter space**, bypassing trajectory generation. WARPD first encodes demonstration trajectories into a latent space, then learns their distribution using a diffusion model, and finally decodes them into policy weights via a hypernetwork [16]. The generated policy is also optimized with model-based imitation learning using a co-trained world (dynamics) model [17], which helps in understanding the environment transitions during training. This approach leverages the success of latent diffusion techniques in vision [50] and language [36], and combines them with learned dynamics models, bringing their advantages to robotic control. The world model, and accompanying loss terms, help the agent learn the optimal policy that can be backpropagated through the learned (differentiable) dynamics, and also apply corrective actions to bring the agent states back into the distribution of the input trajectory dataset. For WARPD, the action horizon corresponds to the number of environment interactions between consecutive policy weight generations. To achieve trajectory encoding and policy parameter decoding, we derive a novel objective function described in Section 3.1, and show that we can approximate its components with a hypernetwork-based VAE and a World Model, and optimize it using a novel loss function described in Section 3.2. This paper provides the following key contributions:

1. **Theoretical Foundations for generating policies:** By integrating concepts from latent diffusion, hypernetworks, and world models, we derive a novel objective function, which when optimized, allows us to generate policy parameters instead of action trajectories.
2. **Longer Action Horizons & Robustness to Perturbations:** By generating closed-loop policies under learned dynamics, WARPD mitigates trajectory tracking errors, enabling policies to operate over extended time horizons with fewer diffusion queries. Additionally, closed-loop policies are reactive to environmental changes, ensuring WARPD-generated policies remain robust under stochastic disturbances.
3. **Lower Inference Costs:** The computational burden of generalization is shifted to the diffusion model, allowing the generated policies to be smaller and more efficient.

We validate these contributions through experiments on the PushT task [10], the Lift and Can tasks from Robomimic [38], and 10 tasks from Metaworld [62]. On Metaworld, WARPD achieves comparable performance to Diffusion Policy but with a  $\sim 45x$  reduction in FLOPs per step, representing a significant improvement in computational efficiency (FLOPs per step are the floating point operations, amortized over all steps of the episode). Analysis across a range of benchmark robotic locomotion and manipulation tasks, demonstrates WARPD’s ability to accurately capture the *behavior distribution* of diverse trajectories, showcasing its capacity to learn a distribution of behaviors.

## 2 Related Work

### 2.1 Imitation Learning and Diffusion for Robotics

Behavioral cloning has progressed with transformer-based models such as PerAct [52] and RT-1 [6], which achieve strong task performance. Vision-language models like RT-2 [5] interpret actions as tokens, while RT-X [11] generalizes across robot embodiments. Object-aware representations [25], energy-based models, and temporal abstraction methods (implicit behavioral cloning [14], sequence compression [65]) improve multitask learning. DBC [8] increases robustness to sensor noise (this is complementary to WARPD, which targets dynamics perturbations such as object shifts or execution-time disturbances). Diffusion models, originally introduced for generative modeling [26, 51], have become powerful tools for robotics. Trajectory-based approaches capture multimodal action distribu-

tions [10], while goal-conditioned methods such as BESO [49] and Latent Diffusion Planning [32] improve efficiency through latent conditioning. Diffusion has also been applied to grasping and motion planning [55, 37, 7], skill chaining [41], and locomotion [30]. Hierarchical extensions including ChainedDiffuser [60], SkillDiffuser [35], and multitask latent diffusion [54] address long-horizon planning. Recently, OCTO [43] demonstrates diffusion-based generalist robot policies.

## 2.2 Hypernetworks and Policy Generation

Hypernetworks, introduced by [16], generate parameters for secondary networks and have been applied in multiple domains. They were first used for meta-learning in one-shot learning tasks [4] and more recently extended to robot policy representations [24]. This direction aligns with Dynamic Filter Networks [31], which emphasize adaptability to input data. Latent Diffusion Models (LDMs) have also been used to model training dynamics in parameter spaces [44]. LDMs have enabled behavior-conditioned policies from text [23] and trajectory embeddings [34], as well as architectures distributions such as ResNets [57]. Unlike [23] and [34], which rely on pre-collected policy datasets, this paper requires a dataset of trajectories.

## 2.3 World Models

[17] introduced world models for forecasting in latent space. PlaNet [19] added pixel-based dynamics learning and online planning. Dreamer [18] learned latent world models with actor-critic RL for long horizons, followed by DreamerV2 [20] with discrete representations achieving human-level Atari, and DreamerV3 [21] scaling across domains. IRIS [39] applied transformers for sequence modeling, reaching superhuman Atari in two hours. SLAC [33] showed stochastic latent variables accelerate RL from high-dimensional inputs. VINs [53] embedded differentiable value iteration for explicit planning, while E2C [58] combined VAEs with locally linear dynamics. DayDreamer [59] enabled real robot learning in one hour, and MILE [28] adapted Dreamer to CARLA with 31% gains. [47] scaled model-based imitation learning to large self-driving datasets. Recent work includes SafeDreamer [64] for safety, STORM [40] with efficient transformers, UniZero [63] for joint model-policy optimization, and Time-Aware World Models [9] capturing temporal dynamics. Beyond these, large-scale pretraining and multimodal foundations extend world models. V-JEPA 2 [1] demonstrated self-supervised video models. DINO-based methods, including Back to the Features [2] and DINO-WM [66], leverage pre-trained visual features. NVIDIA’s Cosmos platform [42] proposes a foundation model ecosystem for physical AI. Vid2World [29] adapts video diffusion models to interactive world modeling, and Pandora [61] integrates natural language actions with video states.

## 3 Method & Problem Formulation

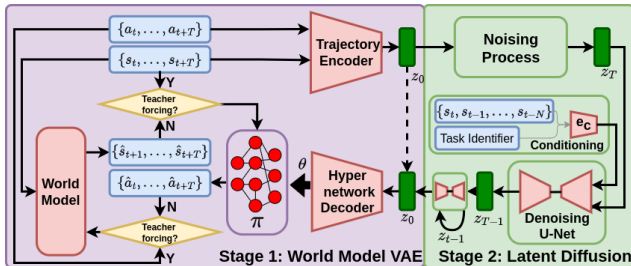


Figure 2: **WARPD**: Stage 1: Pre-train a VAE and world model. The VAE encodes trajectories into a latent space and decodes them as policy parameters, which are optimized for behavior cloning and trajectory tracking. With teacher forcing enabled, the world model is optimized; when disabled, it optimizes the VAE. Stage 2: Train a conditional latent diffusion model to learn the latent distribution.

world model to guide the generated policy to always be in the desired trajectory state distribution. Then, a diffusion model learns the latent distribution (see Figure 2).

Compared to [23], which encodes policy parameters and employs a graph hypernetwork with a MSE loss on parameter reconstruction, our approach differs as it: (1) encodes trajectories as opposed to parameters, into latent space (i.e., we do not require a dataset of policies) (2) uses a simple hypernetwork, (3) applies a behavior cloning loss (detailed in Section 3.1 & Section 3.2) on the

generated policy, and (4) learns a world model for predicting observations given the action in an environment. Below we discuss the problem formulation and derivation.

### 3.1 Latent Policy Representation

We begin by formulating our approach for unconditional policy generation. Assume a distribution over stochastic policies, where variability reflects behavioral diversity. Each policy is parameterized by  $\theta$ , with  $\pi(\cdot, \theta)$  denoting a sampled policy and  $p(\theta)$  the parameter distribution. Sampling a policy corresponds to drawing  $\theta \sim p(\theta)$ . When a policy interacts with the environment, it gives us a trajectory  $\tau = \{s_t, a_t\}_{t=0}^T$ . We assume multiple such trajectories are collected by repeatedly sampling  $\theta$  and executing the corresponding policy. This enables a heterogeneous dataset, e.g., from humans or expert agents. For a given  $\theta$ , actions are noisy:  $a_t \sim \mathcal{N}(\pi(s_t, \theta), \sigma^2)$ .

Our objective is to recover the distribution  $p(\theta)$  that generated the trajectory dataset. We posit a latent variable  $z$  capturing behavioral modes, and assume conditional independence:  $p(\tau | z, \theta) = p(\tau | \theta)$ . Given trajectory data, we maximize the likelihood  $\log p(\tau)$ . To do so, we derive a modified Evidence Lower Bound (mELBO) that incorporates  $p(\theta)$  (see below). This differs from the standard ELBO used in VAEs.

$$\begin{aligned} \log p(\tau) &= \log \int \int p(\tau, \theta, z) dz d\theta \quad (\text{Introduce policy parameter } \theta \text{ and latent variable } z) \\ &= \log \int \int p(\tau | z, \theta) p(\theta | z) p(z) dz d\theta \quad (\text{Apply the chain rule}) \\ &= \log \int \int \frac{p(\tau | z, \theta) p(\theta | z) p(z)}{q(z | \tau)} q(z | \tau) dz d\theta \end{aligned} \quad (1a)$$

(Introduce a variational distribution  $q(z | \tau)$ , approximating the true posterior  $p(z | \tau)$ )

$$= \log \int \mathbb{E}_{p(\theta|z)} \left[ \frac{p(\tau | z, \theta) p(z)}{q(z | \tau)} q(z | \tau) \right] dz \quad (1b)$$

$$\geq \mathbb{E}_{q(z|\tau)} \left[ \log \left( \frac{\mathbb{E}_{p(\theta|z)} [p(\tau | z, \theta)] p(z)}{q(z | \tau)} \right) \right] \quad (\text{Jensen's inequality})$$

$$= \mathbb{E}_{q(z|\tau)} [\log (\mathbb{E}_{p(\theta|z)} [p(\tau | z, \theta)])] - \mathbb{E}_{q(z|\tau)} [\log (q(z | \tau)) - \log (p(z))] \quad (1c)$$

$$= \mathbb{E}_{q(z|\tau)} [\log (\mathbb{E}_{p(\theta|z)} [p(\tau | \theta)])] - \text{KL}(q(z | \tau) \| p(z)) \quad (\text{cond. independence}) \quad (1d)$$

$$\geq \mathbb{E}_{q(z|\tau)} [\mathbb{E}_{p(\theta|z)} [\log (p(\tau | \theta))]] - \text{KL}(q(z | \tau) \| p(z)) \quad (\text{Jensen's inequality}) \quad (1e)$$

Assuming the state transitions are Markov and  $s_1$  is independent of  $\theta$ , the joint likelihood of the entire sequence  $\{(s_1, a_1), (s_2, a_2), \dots, (s_T, a_T)\}$  (i.e.,  $p(\tau | \theta)$ ) is given by:

$$p(s_1, a_1, \dots, s_T, a_T | \theta) = p(s_1) p(a_1 | s_1, \theta) \cdot \prod_{t=2}^T p(s_t | s_{t-1}, a_{t-1}) p(a_t | s_t, \theta) \quad (2a)$$

$$\begin{aligned} \log p(s_1, a_1, \dots, s_T, a_T | \theta) &= \log p(s_1) + \log p(a_1 | s_1, \theta) \\ &\quad + \sum_{t=2}^T [\log p(s_t | s_{t-1}, a_{t-1}) + \log p(a_t | s_t, \theta)] \end{aligned} \quad (2b)$$

Substituting 2b in 1e:

$$\begin{aligned} \log p(\tau) &\geq \mathbb{E}_{q(z|\tau)} [\mathbb{E}_{p(\theta|z)} [\log (p(\tau | \theta))]] - \text{KL}(q(z | \tau) \| p(z)) \\ &= \mathbb{E}_{q(z|\tau)} \left[ \mathbb{E}_{p(\theta|z)} \left[ \sum_{t=1}^T \log p(a_t | s_t, \theta) + \sum_{t=2}^T \log p(s_t | s_{t-1}, a_{t-1}) \right] \right] \\ &\quad - \text{KL}(q(z | \tau) \| p(z)) + A \end{aligned} \quad (3)$$

Where  $A$  consists of  $\log p(s_1)$ , and since this cannot be subject to maximization, we shall ignore it.

Therefore, our modified ELBO is:

$$\mathbb{E}_{q(z|\tau)} \left[ \mathbb{E}_{p(\theta|z)} \left[ \underbrace{\sum_{t=1}^T \log p(a_t | s_t, \theta)}_{\text{Behavior Cloning}} + \underbrace{\sum_{t=2}^T \log p(s_t | s_{t-1}, a_{t-1})}_{\text{World Model}} \right] \right] - \underbrace{\text{KL}(q(z | \tau) \| p(z))}_{\text{KL Regularizer}} \quad (4)$$

### 3.2 Loss function

Since we now have a modified ELBO objective, we shall now try to approximate its components with a variational autoencoder and a world model. Let  $\phi_{enc}$  be the parameters of the VAE encoder that variationally maps trajectories to  $z$ ,  $\phi_{dec}$  be the parameters of the VAE decoder, and  $\phi_{wm}$  be the world model parameters. We assume the latent  $z$  is distributed with mean zero and unit variance. We construct the VAE decoder to approximate  $p(\theta | z)$  with  $p_{\phi_{dec}}(\theta | z)$ . Considering  $a_t \sim \mathcal{N}(\pi(s_t, \theta), \sigma^2)$ , and  $\tau_k = \{s_t^k, a_t^k\}_{t=1}^T$ , we derive our VAE loss function as:

$$\begin{aligned} \mathcal{L}_{BC} &= \sum_{t=1}^T \mathbb{E}_{q_{\phi_{enc}}(z|\tau_k)} [(a_t^k - \pi(s_t^k, f_{\phi_{dec}}(z)))^2] \\ \mathcal{L}_{RO} &= \sum_{t=2}^T \mathbb{E}_{q_{\phi_{enc}}(z|\tau_k)} [\text{KL}(p_{\phi_{wm}}(s_t | s_{t-1}^k, \pi(s_{t-1}^k, f_{\phi_{dec}}(z))) \| p_{\phi_{wm}}(s_t | s_{t-1}^k, a_{t-1}^k))] \\ \mathcal{L}_{TF} &= \sum_{t=2}^T (s_t^k - \hat{s}_t^k)^2 \quad \mathcal{L}_{KL} = \beta_{kl} \sum_{i=1}^{\dim(z)} (\sigma_{e_i}^2 + \mu_{e_i}^2 - 1 - \log \sigma_{e_i}^2) \\ \mathcal{L}(\{s_t^k, a_t^k\}_{t=1}^T | \phi_{enc}, \phi_{dec}, \phi_{wm}) &= \mathcal{L}_{BC} + \mathcal{L}_{RO} + \mathcal{L}_{TF} + \mathcal{L}_{KL} \end{aligned} \quad (5)$$

where,  $\mathcal{L}_{BC}$  is the behavior cloning loss to train the policy decoder,  $\mathcal{L}_{RO}$  is the rollout loss to correct the decoded policy’s actions using the world model,  $\mathcal{L}_{TF}$  is the teacher forcing loss to train the world model, and  $\mathcal{L}_{KL}$  is the KL loss to regularize the latent space.  $\theta$  is obtained from the hypernetwork decoder  $f_{\phi_{dec}}(z)$ .  $(\mu_e, \sigma_e) = f_{\phi_{enc}}(\{s_t^k, a_t^k\}_{t=1}^T)$ ,  $z \sim \mathcal{N}(\mu_e, \sigma_e)$ ,  $\hat{s}_t^k \sim p_{\phi_{wm}}(s_t^k | s_{t-1}^k, a_{t-1}^k)$  and  $\beta_{kl}$  is the regularization weight. The complete derivation is shown in Section A.1. Since the decoder in the VAE outputs the parameter of a secondary network, we shall use a conditional hypernetwork, specifically the model developed for continual learning by [56]. For computational stability, we shall use  $\mathcal{L}_{BC}$ ,  $\mathcal{L}_{RO}$  and  $\mathcal{L}_{KL}$  to optimize the VAE (encoder and decoder parameters) and  $\mathcal{L}_{TF}$  to train the world model parameters. With the teacher forcing objective we get a reliable world model that we can then use in the rollout objective. This is similar to procedures followed in [1, 47, 28]. In practice, we see that approximating  $p(z) = \mathcal{N}(0, I)$  is suboptimal, and therefore we set  $\beta_{kl}$  to a very small number  $\sim (10^{-10}, 10^{-6})$ . After training the VAE to maximize the objective provided in Equation (5) with this  $\beta_{kl}$ , we have access to this latent space  $z$  and can train a diffusion model to learn its distribution  $p(z)$ . We can condition the latent denoising process on the current state and/or the task identifier  $c$  of the policy required. Therefore the model shall be approximating  $p_{\phi_{dif}}(z_{t-1} | z_t, c)$ . After denoising for a given state and task identifier, we can convert the denoised latent to the required policy. Therefore, to sample from  $p(\theta)$ , first sample  $z$  using the trained diffusion model  $z \sim p_{\phi_{dif}}(z_0)$ , and then apply the deterministic function  $f_{\phi_{dec}}$  to the sampled  $z$ . Note that to sample policies during inference, we do not need to encode trajectories; rather, we need to sample a latent using the diffusion model and use the hypernetwork decoder of a pre-trained VAE to decode a policy from it.

## 4 Experiments

We run four sets of experiments. In the first set (Section 4.1), we evaluate the validity of our main contributions. In the second set (Section 4.2), we ablate different components of our method. In the third set (Section 4.3), we show how WARPDP can be scaled to vision-based observation environments. In the final set (Section 4.4), we analyze the behavior distribution modeled by our latent space. In the first set, we compare WARPDP with action trajectory generation methods with respect to 1) Longer Action Horizons and Environment Perturbations, where experiments are performed while varying these parameters on the PushT task [10] and the Lift and Can Robomimic tasks [38], and 2) Lower inference costs, where experiments are performed on 10 tasks from the Metaworld [62] suite of tasks, to show WARPDP requires fewer parameters during inference while maintaining multi-task performance. The task descriptions are provided in Section A.5. We choose a multi-task experiment here as the model capacity required for solving multiple tasks generally increases with the number of tasks.

We focus on demonstrating results in state-based observation spaces. Our generated policies are Multi-Layer Perceptrons (MLP) with 2 hidden layers with 256 neurons each. In the VAE, the encoder is a sequential network that flattens the trajectory and compresses it to a low-dimensional latent space, and the decoder is a conditional hypernetwork [13]. The details of the VAE implementation are

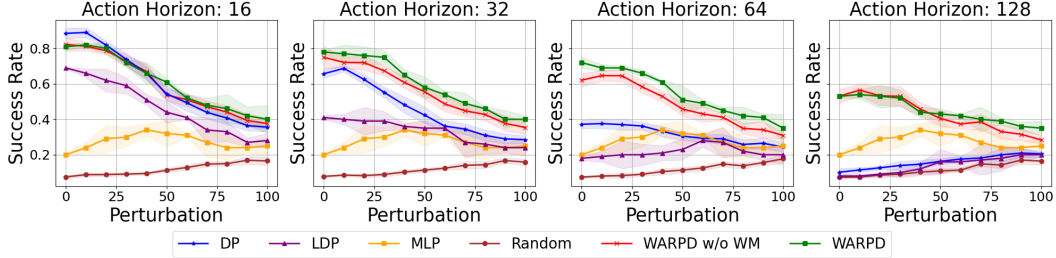


Figure 3: **Longer action horizons and robustness to perturbations on PushT:** Performance of WARPDP and baselines on the PushT task as we vary the action horizons and environment perturbations.

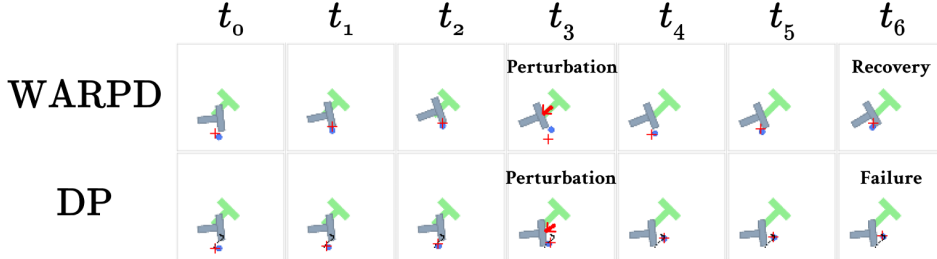


Figure 4: **Visualization of Perturbation:** When an adversarial perturbation is applied, we see that WARPDP’s generated closed-loop policy successfully adapts to the change.

provided in Section A.8.2 and Section A.8.3. For the world model, since we use low-dimensional observation spaces, we use a simple MLP with 2 hidden layers with 1024 neurons each to map the history of observations and actions to the next observation. For stability, we use  $\mathcal{L}_{RO}$  only after 10 epochs of training. This warm-starts the world model before we use it to optimize the policy generator. For all experiments, the latent space is  $\mathbb{R}^{256}$  and the learning rate is  $10^{-4}$  with the Adam optimizer. For the diffusion model, we use the DDPM Scheduler for denoising. Based on the results are shown in Section A.3 (inspired by [10]), we chose the ConditionalUnet1D model for all experiments in the paper. Just as [10], we condition the diffusion model with FiLM layers, and also use the Exponential Moving Average [22] of parameter weights (commonly used in DDPM) for stability. All results presented are obtained over three seeds, and the compute resources are described in Section A.9

## 4.1 Empirical Evaluation of Contributions

### 4.1.1 Longer Action Horizons & Robustness to Perturbations

We first evaluate our method on the PushT task [10], a standard benchmark for diffusion-based trajectory generation in manipulation. The goal is to align a ‘T’ block with a target position and orientation on a 2D surface. Observations consist of the end-effector’s position and the block’s position and orientation. Actions specify the end-effector’s target position at each time step. Success rate is defined as the maximum overlap between the actual and desired block poses during a rollout. We test under different action horizons and varying levels of environment perturbation, simulated via an adversarial agent that randomly displaces the ‘T’ block.

For the WARPDP model, we first train a VAE to encode trajectory snippets (of length equal to the action horizon) into latents representing locally optimal policies. These policies are optimized with a co-trained world model. A conditional latent diffusion model, given the current state, then generates a latent that the VAE decoder transforms into a locally optimal policy for the next action horizon. The inference process is illustrated in Figure 1. We train two variants of WARPDP, with (WARPDP) and without (WARPDP w/o WM) the world model (i.e., we train WARPDP with just  $\mathcal{L}_{BC} + \mathcal{L}_{KL}$ ).

As baselines for this experiment, we compare the proposed WARPDP variants against four alternatives: 1) a **Diffusion Policy (DP)** model that generates open-loop action trajectories for a fixed action horizon; 2) a **Latent Diffusion Policy (LDP)** model, which is structurally similar to WARPDP but decodes the latent representation into an action trajectory rather than a closed-loop policy; 3) a **Multilayer Perceptron (MLP)** policy, which shares the same architecture as the policy network generated by WARPDP and serves to isolate the impact of diffusion modeling; 4) a **Random Policy**, which provides a lower-bound performance reference. For a fair comparison, all diffusion-based models (WARPDP, DP, and LDP) use the same diffusion model size and hyperparameters, corresponding to the medium

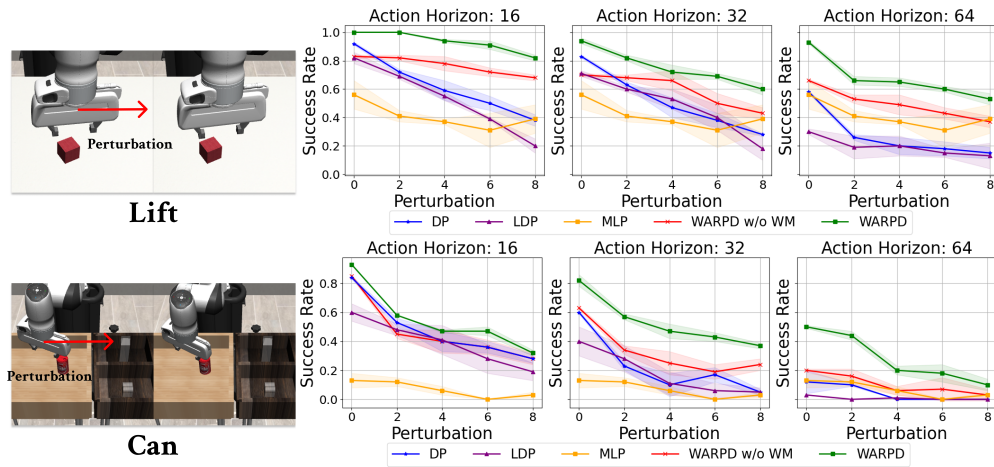


Figure 5: **Longer action horizons and robustness to perturbations on Robomimic tasks:** Performance of WARP and DP as we vary the action horizon and environment perturbations.

configuration described in Section A.8.4 and Section A.8.7. LDP uses a VAE decoder, implemented as an MLP with two hidden layers of 256 neurons each, to output an action chunk of the same length as the action horizon.

All models are evaluated across 50 uniquely seeded environment instances, with each evaluation repeated 10 times, across 3 training seeds. Figure 3 illustrates the impact of perturbation magnitudes and action horizons on success rates across all baselines. Perturbations refer to random displacements applied to the T block, occurring at randomly selected time steps with 10% probability. A sample rollout with a perturbation magnitude of 50 is shown in Figure 4.

While DP demonstrates comparable performance to both WARP variants at an action horizon of 16 with minimal perturbations, WARP exhibits superior robustness as the action horizon increases. This enhanced robustness of WARP with the world model becomes more pronounced in the presence of larger perturbations. Specifically, at longer action horizons such as 128, WARP w/ WM maintains a significantly higher success rate compared to DP across all perturbation levels. The MLP generally underperforms compared to both WARP variants and DP, highlighting the benefits of diffusion-based approaches for this task. LDP has a lower success rate than WARP, indicating that generating a closed-loop policy is more important than learning the latent representation space. The relatively lower sensitivity to perturbations at an action horizon of 16 for both policies can be attributed to the more frequent action trajectory queries inherent in DP at shorter horizons (i.e. smaller action chunks), effectively approximating a more closed-loop control strategy.

We also ran experiments on the Robomimic [38] Lift and Can tasks, using the same hyperparameters as the PushT experiment, the same task settings, and the mh demonstration data from [10]. To simulate perturbations, we add random translation and rotation vectors to the end effector, applied 10% of the time. Figure 5 shows the performance of the WARP variants and baselines under these perturbations across different action horizons. The x-axis corresponds to perturbation magnitude. Similar to PushT, WARP outperforms DP for longer horizons and is more robust to perturbations. Here, we see that WARP also significantly outperforms WARP w/o WM. We believe that this is because the state density of the provided dataset is higher in PushT as compared to Robomimic, and model-based imitation learning (with the world model) provides robustness to covariate shift [47, 28].

#### 4.1.2 Low Inference Cost

We will now look at the next contribution, namely, lower inference cost compared to methods that diffuse action trajectories instead of policies. When training a single policy on multiple tasks, it is known that a larger model capacity is needed. This is detrimental in robotics applications as this increases control latency. We train a task-conditioned WARP model and show that the cost of task generalization is borne by the latent diffusion model, **while the generated execution policy remains small**. Because WARP generates a smaller policy, the runtime compute required for inference is lower than SOTA diffusion methods.

We experiment on 10 tasks of the Metaworld benchmark, the details of which are in Section A.5. We set the action horizon to the length of the entire trajectory for WARPD to generate policies that shall work for the entire duration of the rollout, where at each time step, the generated MLPs shall predict instantaneous control. We experimented over three sizes of the generated MLP policy: 128, 256, and 512 neurons per layer, each having 2 hidden layers. We also train 10 DP models, spread over a grid of 5 different sizes (xs, s, m, l, xl) and 2 action horizons: 32 and 128. Each DP model is run at an inference frequency of half the action horizon. We provide the details of the DP model in Section A.8.1. Finally, we also train 3 MLP models with 128, 256, and 512 neurons per layer, as baselines.

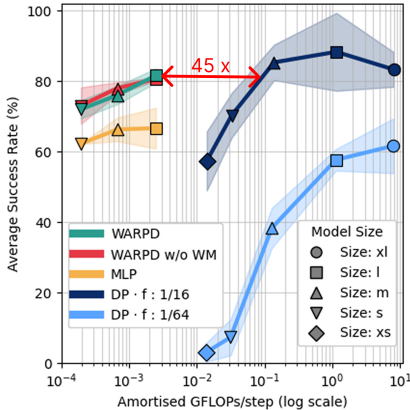


Figure 6: **Success rate vs. average compute** of WARPD, DP, and MLP policies on 10 Metaworld tasks for various model sizes. The x-axis shows the GFLOPs/step for each policy on a log scale. WARPD performs  $\sim 45\times$  fewer inference computations than a DP policy with comparable performance.

the w/o WM variant. In different scenarios, such as the state-conditioned experiments where the policy is regenerated more frequently, the generation cost could also be amortized. Even in such a conservative setting, when we incorporate the computational cost for generation (0.0227 GFLOPs), WARPD still requires  $\sim 4.5\times$  fewer inference operations.

## 4.2 Ablations

Considering that WARPD consists of multiple components, we analyze each one. We perform ablations over three components of our method: 1) Diffusion model architecture, Section A.3; 2) VAE decoder size, Section A.4; 3) KL coefficient for the VAE, Section A.4.1. We find that: 1) a UNET converges faster than a transformer, 2) using a larger hypernetwork decoder increases the performance, 3) using a lower KL coefficient generates policies that better track a desired trajectory. Further, in Section 4.1.1, we ablate the world model and see that it helps more in the Robomimic tasks than in the PushT task. We believe this is because the state space is more complex in Robomimic than that in PushT, whilst the number of trajectories remains roughly the same. This results in insufficient trajectories covering the state space, rendering the learned policy susceptible to covariate shift.

## 4.3 Vision Observation Scaling

We conducted initial experiments on the PushT image environment to evaluate the applicability of our method in vision-based tasks. Our approach involved pre-training a vision encoder to map images of the PushT environment to their corresponding ground truth states. We then trained WARPD to utilize these image embeddings as states. For

Note that WARPD uses a fixed action horizon equal to the full episode length (500 steps), whereas the DP model uses a variable horizon. The WARPD inference process is illustrated on the right-hand side of Figure 1. All baseline models receive the task identifier as part of the state input. Each model is trained with 3 random seeds, and evaluated across 10 tasks, with 16 rollouts per task. Figure 6 presents the results of this evaluation. In the plot, the x-axis represents average per-step inference compute (in GFLOPs), and the y-axis indicates the overall success rate across tasks. For DP models, achieving high success rates requires increasing model size or denoising frequency (i.e., predicting shorter action chunks), both of which raise computational cost. In contrast, WARPD generates a simpler, more efficient controller, requiring significantly less compute. The best-performing WARPD model achieves an 81% success rate with  $\sim 45\times$  fewer inference operations than the closest-performing DP model. Interestingly, the MLP baseline also performs well, and is comparable in efficiency to WARPD, but still lags in performance. We attribute this to the unimodal nature of this dataset, as MLPs struggled with the multimodal PushT task in the previous section. Note that the WARPD performed comparably to

Perturbation	WARPD	DP
0	0.54 $\pm$ 0.05	<b>0.57 <math>\pm</math> 0.05</b>
20	<b>0.53 <math>\pm</math> 0.01</b>	0.50 $\pm$ 0.05
40	<b>0.45 <math>\pm</math> 0.01</b>	0.42 $\pm$ 0.05
60	<b>0.41 <math>\pm</math> 0.08</b>	0.34 $\pm$ 0.02
80	<b>0.36 <math>\pm</math> 0.06</b>	0.30 $\pm$ 0.02
100	<b>0.28 <math>\pm</math> 0.05</b>	0.24 $\pm$ 0.06

Table 1: **PushT Image results** with horizon 64

comparison, we also trained a Diffusion Policy (DP) model on the same embeddings. The results for an action horizon of 64 are presented below.

As shown in Table 1, WARPD consistently outperforms DP in the presence of increasing perturbation, demonstrating its robustness even when operating on image-derived state embeddings. These experiments strongly suggest that if an effective image embedding can be learned, the low-dimensional state space version of WARPD is readily applicable to vision-based tasks. This serves as an encouraging proof-of-concept for WARPD’s generalizability beyond state-based environments. It can be noted here as well that a diffusion model’s inference cost ( $\sim 3.99$  GFLOPs) is still much greater than the hypernetwork decoder ( $\sim 0.056$  GFLOPs) and the ResNet18 vision encoder ( $\sim 0.334$  GFLOPs)

#### 4.4 Behavior Analysis

WARPD models trajectory data from a distribution of policies, exposing this distribution through its latent space. On the Robomimic Lift task with the MH dataset (300 trajectories from 6 operators of varied proficiency: 2 “worse,” 2 “okay,” and 2 “better.”), WARPD encoded entire demonstration trajectories. A 2D t-SNE plot revealed clusters aligned with operator identity, despite WARPD receiving no explicit operator labels. This shows WARPD can cluster behaviors and potentially filter unwanted ones. This is further studied in Section A.7.

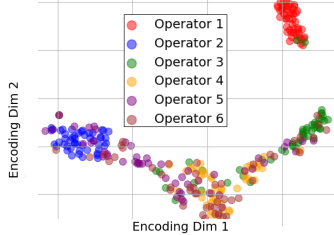


Figure 7: Behavior distribution

### 5 Limitations and Future Work

While WARPD is a promising framework for policy generation, Diffusion Policy (DP) performs better in short-horizon, low-perturbation settings. This gap likely stems from VAE approximation errors and WARPD’s added complexity. Another limitation is the additional training overhead compared to traditional diffusion policy models (see Section A.9). But we believe that this training overhead is comparable to other established world model-based imitation learning methods.

Thus, future work could improve WARPD’s VAE decoder through chunked deconvolutional hypernetworks [56], enabling more efficient decoding. Extending WARPD to Transformer or ViT policies is another direction, especially for sequential or visual tasks [12]. Incorporating WARPD to foundation VLA models as an action head is another exciting avenue. Finally, warm-starting with prior latents [10] may further boost performance by providing richer priors.

### 6 Conclusion

We introduce World Model Assisted Reactive Policy Diffusion (WARPD), a novel framework for learning a distribution over policies from diverse demonstration trajectories. WARPD models behavioral diversity via latent diffusion, a world model, and uses a hypernetwork decoder to generate policy weights, enabling closed-loop control directly from sampled latents. Our evaluation highlights two key strengths of WARPD: robustness and computational efficiency. Compared to Diffusion Policy, WARPD delivers more reliable performance in environments with long action horizons and perturbations, while reducing inference costs, especially in multi-task settings.

## References

- [1] Mido Assran, Adrien Bardes, David Fan, Quentin Garrido, Russell Howes, Matthew Muckley, Ammar Rizvi, Claire Roberts, Koustuv Sinha, Artem Zholus, et al. V-jepa 2: Self-supervised video models enable understanding, prediction and planning. *arXiv preprint arXiv:2506.09985*, 2025.
- [2] Federico Baldassarre, Marc Szafraniec, Basile Terver, Vasil Khalidov, Francisco Massa, Yann LeCun, Patrick Labatut, Maximilian Seitzer, and Piotr Bojanowski. Back to the features: Dino as a foundation for video world models, 2025.
- [3] Sumeet Batra, Bryon Tjanaka, Matthew C Fontaine, Aleksei Petrenko, Stefanos Nikolaidis, and Gaurav Sukhatme. Proximal policy gradient arborescence for quality diversity reinforcement learning. *arXiv preprint arXiv:2305.13795*, 2023.
- [4] Luca Bertinetto, João F. Henriques, Jack Valmadre, Philip Torr, and Andrea Vedaldi. Learning feed-forward one-shot learners. In D. Lee, M. Sugiyama, U. Luxburg, I. Guyon, and R. Garnett, editors, *Advances in Neural Information Processing Systems*, volume 29. Curran Associates, Inc., 2016.
- [5] Anthony Brohan, Noah Brown, Justice Carbajal, Yevgen Chebotar, Xi Chen, Krzysztof Choro-manski, Tianli Ding, Danny Driess, Avinava Dubey, Chelsea Finn, Pete Florence, Chuyuan Fu, Montse Gonzalez Arenas, Keerthana Gopalakrishnan, Kehang Han, Karol Hausman, Alex Herzog, Jasmine Hsu, Brian Ichter, Alex Irpan, Nikhil Joshi, Ryan Julian, Dmitry Kalashnikov, Yuheng Kuang, Isabel Leal, Lisa Lee, Tsang-Wei Edward Lee, Sergey Levine, Yao Lu, Henryk Michalewski, Igor Mordatch, Karl Pertsch, Kanishka Rao, Krista Reymann, Michael Ryoo, Grecia Salazar, Pannag Sanketi, Pierre Sermanet, Jaspier Singh, Anikait Singh, Radu Soricut, Huang Tran, Vincent Vanhoucke, Quan Vuong, Ayzaan Wahid, Stefan Welker, Paul Wohlhart, Jialin Wu, Fei Xia, Ted Xiao, Peng Xu, Sichun Xu, Tianhe Yu, and Brianna Zitkovich. Rt-2: Vision-language-action models transfer web knowledge to robotic control. In *arXiv preprint arXiv:2307.15818*, 2023.
- [6] Anthony Brohan, Noah Brown, Justice Carbajal, Yevgen Chebotar, Joseph Dabis, Chelsea Finn, Keerthana Gopalakrishnan, Karol Hausman, Alex Herzog, Jasmine Hsu, Julian Ibarz, Brian Ichter, Alex Irpan, Tomas Jackson, Sally Jesmonth, Nikhil Joshi, Ryan Julian, Dmitry Kalashnikov, Yuheng Kuang, Isabel Leal, Kuang-Huei Lee, Sergey Levine, Yao Lu, Utsav Malla, Deeksha Manjunath, Igor Mordatch, Ofir Nachum, Carolina Parada, Jodilyn Peralta, Emily Perez, Karl Pertsch, Jornell Quiambao, Kanishka Rao, Michael Ryoo, Grecia Salazar, Pannag Sanketi, Kevin Sayed, Jaspier Singh, Sumedh Sontakke, Austin Stone, Clayton Tan, Huang Tran, Vincent Vanhoucke, Steve Vega, Quan Vuong, Fei Xia, Ted Xiao, Peng Xu, Sichun Xu, Tianhe Yu, and Brianna Zitkovich. Rt-1: Robotics transformer for real-world control at scale. In *arXiv preprint arXiv:2212.06817*, 2022.
- [7] Joao Carvalho, An T Le, Mark Baierl, Dorothea Koert, and Jan Peters. Motion planning diffusion: Learning and planning of robot motions with diffusion models. in 2023 *IEEE International Conference on Intelligent Robots and Systems (IROS)*, pages 1916–1923.
- [8] Shang-Fu Chen, Hsiang-Chun Wang, Ming-Hao Hsu, Chun-Mao Lai, and Shao-Hua Sun. Diffusion model-augmented behavioral cloning. In *International Conference on Machine Learning*, pages 7486–7510. PMLR, 2024.
- [9] Yixuan Chen, Hao Zhang, and Jian Liu. Time-aware world model for adaptive prediction and control. *arXiv preprint arXiv:2506.08441*, 2025.
- [10] Cheng Chi, Zhenjia Xu, Siyuan Feng, Eric Cousineau, Yilun Du, Benjamin Burchfiel, Russ Tedrake, and Shuran Song. Diffusion policy: Visuomotor policy learning via action diffusion. *The International Journal of Robotics Research*, 2024.
- [11] Open X-Embodiment Collaboration, Abby O’Neill, Abdul Rehman, Abhinav Gupta, Abhiram Maddukuri, Abhishek Gupta, Abhishek Padalkar, Abraham Lee, Acorn Pooley, Agrim Gupta, Ajay Mandlekar, Ajinkya Jain, Albert Tung, Alex Bewley, Alex Herzog, Alex Irpan, Alexander Khazatsky, Anant Rai, Anchit Gupta, Andrew Wang, Andrey Kolobov, Anikait

Singh, Animesh Garg, Aniruddha Kembhavi, Annie Xie, Anthony Brohan, Antonin Raffin, Archit Sharma, Arefeh Yavary, Arhan Jain, Ashwin Balakrishna, Ayzaan Wahid, Ben Burgess-Limerick, Beomjoon Kim, Bernhard Schölkopf, Blake Wulfe, Brian Ichter, Cewu Lu, Charles Xu, Charlotte Le, Chelsea Finn, Chen Wang, Chenfeng Xu, Cheng Chi, Chenguang Huang, Christine Chan, Christopher Agia, Chuer Pan, Chuyuan Fu, Coline Devin, Danfei Xu, Daniel Morton, Danny Driess, Daphne Chen, Deepak Pathak, Dhruv Shah, Dieter Buechler, Dinesh Jayaraman, Dmitry Kalashnikov, Dorsa Sadigh, Edward Johns, Ethan Foster, Fangchen Liu, Federico Ceola, Fei Xia, Feiyu Zhao, Felipe Vieira Frujeri, Freek Stulp, Gaoyue Zhou, Gaurav S. Sukhatme, Gautam Salhotra, Ge Yan, Gilbert Feng, Giulio Schiavi, Glen Berseth, Gregory Kahn, Guangwen Yang, Guanzhi Wang, Hao Su, Hao-Shu Fang, Haochen Shi, Henghui Bao, Heni Ben Amor, Henrik I Christensen, Hiroki Furuta, Homanga Bharadhwaj, Homer Walke, Hongjie Fang, Huy Ha, Igor Mordatch, Ilija Radosavovic, Isabel Leal, Jacky Liang, Jad Abou-Chakra, Jaehyung Kim, Jaimyn Drake, Jan Peters, Jan Schneider, Jasmine Hsu, Jay Vakil, Jeannette Bohg, Jeffrey Bingham, Jeffrey Wu, Jensen Gao, Jiaheng Hu, Jiajun Wu, Jialin Wu, Jiankai Sun, Jianlan Luo, Jiayuan Gu, Jie Tan, Jihoon Oh, Jimmy Wu, Jingpei Lu, Jingyun Yang, Jitendra Malik, João Silvério, Joey Hejna, Jonathan Boother, Jonathan Tompson, Jonathan Yang, Jordi Salvador, Joseph J. Lim, Junhyek Han, Kaiyuan Wang, Kanishka Rao, Karl Pertsch, Karol Hausman, Keegan Go, Keerthana Gopalakrishnan, Ken Goldberg, Kendra Byrne, Kenneth Oslund, Kento Kawaharazuka, Kevin Black, Kevin Lin, Kevin Zhang, Kiana Ehsani, Kiran Lekkala, Kirsty Ellis, Krishan Rana, Krishnan Srinivasan, Kuan Fang, Kunal Pratap Singh, Kuo-Hao Zeng, Kyle Hatch, Kyle Hsu, Laurent Itti, Lawrence Yunliang Chen, Lerrel Pinto, Li Fei-Fei, Liam Tan, Linxi "Jim" Fan, Lionel Ott, Lisa Lee, Luca Weihs, Magnum Chen, Marion Lepert, Marius Memmel, Masayoshi Tomizuka, Masha Itkina, Mateo Guaman Castro, Max Spero, Maximilian Du, Michael Ahn, Michael C. Yip, Mingtong Zhang, Mingyu Ding, Minh Heo, Mohan Kumar Srirama, Mohit Sharma, Moo Jin Kim, Naoaki Kanazawa, Nicklas Hansen, Nicolas Heess, Nikhil J Joshi, Niko Suenderhauf, Ning Liu, Norman Di Palo, Nur Muhammad Mahi Shafiullah, Oier Mees, Oliver Kroemer, Osbert Bastani, Pannag R Sanketi, Patrick "Tree" Miller, Patrick Yin, Paul Wohlhart, Peng Xu, Peter David Fagan, Peter Mitrano, Pierre Sermanet, Pieter Abbeel, Priya Sundaesan, Qiuyu Chen, Quan Vuong, Rafael Rafailov, Ran Tian, Ria Doshi, Roberto Mart'in-Mart'in, Rohan Bajjal, Rosario Scalise, Rose Hendrix, Roy Lin, Runjia Qian, Ruohan Zhang, Russell Mendonca, Rutav Shah, Ryan Hoque, Ryan Julian, Samuel Bustamante, Sean Kirmani, Sergey Levine, Shan Lin, Sherry Moore, Shikhar Bahl, Shivin Dass, Shubham Sonawani, Shubham Tulsiani, Shuran Song, Sichun Xu, Siddhant Halder, Siddharth Karamcheti, Simeon Adebola, Simon Guist, Soroush Nasiriany, Stefan Schaal, Stefan Welker, Stephen Tian, Subramanian Ramamoorthy, Sudeep Dasari, Suneel Belkhale, Sungjae Park, Suraj Nair, Suvir Mirchandani, Takayuki Osa, Tanmay Gupta, Tatsuya Harada, Tatsuya Matsushima, Ted Xiao, Thomas Kollar, Tianhe Yu, Tianli Ding, Todor Davchev, Tony Z. Zhao, Travis Armstrong, Trevor Darrell, Trinity Chung, Vidhi Jain, Vikash Kumar, Vincent Vanhoucke, Wei Zhan, Wenxuan Zhou, Wolfram Burgard, Xi Chen, Xiangyu Chen, Xiaolong Wang, Xinghao Zhu, Xinyang Geng, Xiyuan Liu, Xu Liangwei, Xuanlin Li, Yansong Pang, Yao Lu, Yecheng Jason Ma, Yejin Kim, Yevgen Chebotar, Yifan Zhou, Yifeng Zhu, Yilin Wu, Ying Xu, Yixuan Wang, Yonatan Bisk, Yongqiang Dou, Yoonyoung Cho, Youngwoon Lee, Yuchen Cui, Yue Cao, Yueh-Hua Wu, Yujin Tang, Yuke Zhu, Yunchu Zhang, Yunfan Jiang, Yunshuang Li, Yunzhu Li, Yusuke Iwasawa, Yutaka Matsuo, Zehan Ma, Zhuo Xu, Zichen Jeff Cui, Zichen Zhang, Zipeng Fu, and Zipeng Lin. Open X-Embodiment: Robotic learning datasets and RT-X models. <https://arxiv.org/abs/2310.08864>, 2023.

- [12] Alexey Dosovitskiy, Lucas Beyer, Alexander Kolesnikov, Dirk Weissenborn, Xiaohua Zhai, Thomas Unterthiner, Mostafa Dehghani, Matthias Minderer, Georg Heigold, Sylvain Gelly, Jakob Uszkoreit, and Neil Houlsby. An image is worth 16x16 words: Transformers for image recognition at scale. *CoRR*, abs/2010.11929, 2020.
- [13] Benjamin Ehret, Christian Henning, Maria R. Cervera, Alexander Meulemans, Johannes von Oswald, and Benjamin F. Grewe. Continual learning in recurrent neural networks. In *International Conference on Learning Representations*, 2021.
- [14] Pete Florence, Corey Lynch, Andy Zeng, Oscar A Ramirez, Ayzaan Wahid, Laura Downs, Adrian Wong, Johnny Lee, Igor Mordatch, and Jonathan Tompson. Implicit behavioral cloning. In Aleksandra Faust, David Hsu, and Gerhard Neumann, editors, *Proceedings of the 5th*

- Conference on Robot Learning*, volume 164 of *Proceedings of Machine Learning Research*, pages 158–168. PMLR, 08–11 Nov 2022.
- [15] Justin Fu, Aviral Kumar, Ofir Nachum, George Tucker, and Sergey Levine. D4rl: Datasets for deep data-driven reinforcement learning, 2020.
  - [16] David Ha, Andrew Dai, and Quoc V Le. Hypernetworks. *arXiv preprint arXiv:1609.09106*, 2016.
  - [17] David Ha and Jürgen Schmidhuber. Recurrent world models facilitate policy evolution. In *Advances in Neural Information Processing Systems 31*, pages 2451–2463. Curran Associates, Inc., 2018. <https://worldmodels.github.io>.
  - [18] Danijar Hafner, Timothy Lillicrap, Jimmy Ba, and Mohammad Norouzi. Dream to control: Learning behaviors by latent imagination. *arXiv preprint arXiv:1912.01603*, 2019.
  - [19] Danijar Hafner, Timothy Lillicrap, Ian Fischer, Ruben Villegas, David Ha, Honglak Lee, and James Davidson. Learning latent dynamics for planning from pixels. *arXiv preprint arXiv:1811.04551*, 2019.
  - [20] Danijar Hafner, Timothy Lillicrap, Ian Fischer, Ruben Villegas, David Ha, Honglak Lee, and James Davidson. Mastering atari with discrete world models. *arXiv preprint arXiv:2010.02193*, 2020.
  - [21] Danijar Hafner, Jurgis Pašukonis, Jimmy Ba, and Timothy Lillicrap. Mastering diverse domains through world models. *arXiv preprint arXiv:2301.04104*, 2023.
  - [22] Kaiming He, Haoqi Fan, Yuxin Wu, Saining Xie, and Ross Girshick. Momentum contrast for unsupervised visual representation learning. In *Proceedings of the IEEE/CVF conference on computer vision and pattern recognition*, pages 9729–9738, 2020.
  - [23] Shashank Hegde, Sumeet Batra, KR Zentner, and Gaurav Sukhatme. Generating behaviorally diverse policies with latent diffusion models. *Advances in Neural Information Processing Systems*, 36:7541–7554, 2023.
  - [24] Shashank Hegde, Zhehui Huang, and Gaurav S Sukhatme. Hyperppo: A scalable method for finding small policies for robotic control. In *2024 IEEE International Conference on Robotics and Automation (ICRA)*, pages 10821–10828. IEEE, 2024.
  - [25] Negin Heravi, Ayzaan Wahid, Corey Lynch, Peter R. Florence, Travis Armstrong, Jonathan Tompson, Pierre Sermanet, Jeannette Bohg, and Debidatta Dwibedi. Visuomotor control in multi-object scenes using object-aware representations. *2023 IEEE International Conference on Robotics and Automation (ICRA)*, pages 9515–9522, 2022.
  - [26] Jonathan Ho, Ajay Jain, and Pieter Abbeel. Denoising diffusion probabilistic models. In Hugo Larochelle, Marc’Aurelio Ranzato, Raia Hadsell, Maria-Florina Balcan, and Hsuan-Tien Lin, editors, *Advances in Neural Information Processing Systems 33: Annual Conference on Neural Information Processing Systems 2020, NeurIPS 2020, December 6-12, 2020, virtual*, 2020.
  - [27] Jonathan Ho, Ajay Jain, and Pieter Abbeel. Denoising diffusion probabilistic models. *Advances in neural information processing systems*, 33:6840–6851, 2020.
  - [28] Anthony Hu, Zak Murez, Nikhil Mohan, Sofia Dudas, Jeffrey Hawke, Vijay Badrinarayanan, Roberto Cipolla, and Alex Kendall. Model-based imitation learning for urban driving. *arXiv preprint arXiv:2210.07729*, 2022.
  - [29] Siqiao Huang, Jialong Wu, Qixing Zhou, Shangchen Miao, and Mingsheng Long. Vid2world: Crafting video diffusion models to interactive world models, 2025.
  - [30] Xiaoyu Huang, Yufeng Chi, Ruofeng Wang, Zhongyu Li, Xue Bin Peng, Sophia Shao, Borivoje Nikolic, and Koushil Sreenath. Diffuseloco: Real-time legged locomotion control with diffusion from offline datasets. *arXiv preprint arXiv:2404.19264*, 2024.

- [31] Xu Jia, Bert De Brabandere, Tinne Tuytelaars, and Luc V Gool. Dynamic filter networks. In D. Lee, M. Sugiyama, U. Luxburg, I. Guyon, and R. Garnett, editors, *Advances in Neural Information Processing Systems*, volume 29. Curran Associates, Inc., 2016.
- [32] Deqian Kong, Dehong Xu, Minglu Zhao, Bo Pang, Jianwen Xie, Andrew Lizarraga, Yuhao Huang, Sirui Xie, and Ying Nian Wu. Latent plan transformer for trajectory abstraction: Planning as latent space inference. *Advances in Neural Information Processing Systems*, 37:123379–123401, 2024.
- [33] Alex X Lee, Anusha Nagabandi, Pieter Abbeel, and Sergey Levine. Stochastic latent actor-critic: Deep reinforcement learning with a latent variable model. *arXiv preprint arXiv:1907.00953*, 2019.
- [34] Yongyuan Liang, Tingqiang Xu, Kaizhe Hu, Guangqi Jiang, Furong Huang, and Huazhe Xu. Make-an-agent: A generalizable policy network generator with behavior-prompted diffusion. *arXiv preprint arXiv:2407.10973*, 2024.
- [35] Zhixuan Liang, Yao Mu, Hengbo Ma, Masayoshi Tomizuka, Mingyu Ding, and Ping Luo. Skilldiffuser: Interpretable hierarchical planning via skill abstractions in diffusion-based task execution. In *Proceedings of the IEEE/CVF Conference on Computer Vision and Pattern Recognition*, pages 16467–16476, 2024.
- [36] Justin Lovelace, Varsha Kishore, Chao Wan, Eliot Shekhtman, and Kilian Q Weinberger. Latent diffusion for language generation. *Advances in Neural Information Processing Systems*, 36, 2024.
- [37] Yunhao Luo, Chen Sun, Joshua B Tenenbaum, and Yilun Du. Potential based diffusion motion planning. *arXiv preprint arXiv:2407.06169*, 2024.
- [38] Ajay Mandlekar, Danfei Xu, Josiah Wong, Soroush Nasiriany, Chen Wang, Rohun Kulkarni, Li Fei-Fei, Silvio Savarese, Yuke Zhu, and Roberto Martín-Martín. What matters in learning from offline human demonstrations for robot manipulation. In *arXiv preprint arXiv:2108.03298*, 2021.
- [39] Vincent Micheli, Eloi Alonso, and François Fleuret. Transformers are sample-efficient world models. In *International Conference on Learning Representations*, 2023.
- [40] Vincent Micheli, Eloi Alonso, and François Fleuret. Storm: Efficient stochastic transformer based world models for reinforcement learning. *arXiv preprint arXiv:2310.09615*, 2024.
- [41] Utkarsh Aashu Mishra, Shangjie Xue, Yongxin Chen, and Danfei Xu. Generative skill chaining: Long-horizon skill planning with diffusion models. In *Conference on Robot Learning*, 2023.
- [42] NVIDIA, :, Niket Agarwal, Arslan Ali, Maciej Bala, Yogesh Balaji, Erik Barker, Tiffany Cai, Prithvijit Chattopadhyay, Yongxin Chen, Yin Cui, Yifan Ding, Daniel Dworakowski, Jiaojiao Fan, Michele Fenzi, Francesco Ferroni, Sanja Fidler, Dieter Fox, Songwei Ge, Yunhao Ge, Jinwei Gu, Siddharth Gururani, Ethan He, Jiahui Huang, Jacob Huffman, Pooya Jannaty, Jingyi Jin, Seung Wook Kim, Gergely Klár, Grace Lam, Shiyi Lan, Laura Leal-Taixe, Anqi Li, Zhaoshuo Li, Chen-Hsuan Lin, Tsung-Yi Lin, Huan Ling, Ming-Yu Liu, Xian Liu, Alice Luo, Qianli Ma, Hanzi Mao, Kaichun Mo, Arsalan Mousavian, Seungjun Nah, Sriharsha Niverty, David Page, Despoina Paschalidou, Zeeshan Patel, Lindsey Pavao, Morteza Ramezani, Fitsum Reda, Xiaowei Ren, Vasanth Rao Naik Sabavat, Ed Schmerling, Stella Shi, Bartosz Stefaniak, Shitao Tang, Lyne Tchapmi, Przemek Tredak, Wei-Cheng Tseng, Jibin Varghese, Hao Wang, Haoxiang Wang, Heng Wang, Ting-Chun Wang, Fangyin Wei, Xinyue Wei, Jay Zhangjie Wu, Jiashu Xu, Wei Yang, Lin Yen-Chen, Xiaohui Zeng, Yu Zeng, Jing Zhang, Qinsheng Zhang, Yuxuan Zhang, Qingqing Zhao, and Artur Zolkowski. Cosmos world foundation model platform for physical ai, 2025.
- [43] Octo Model Team, Dibya Ghosh, Homer Walke, Karl Pertsch, Kevin Black, Oier Mees, Sudeep Dasari, Joey Hejna, Charles Xu, Jianlan Luo, Tobias Kreiman, You Liang Tan, Lawrence Yunliang Chen, Pannag Sanketi, Quan Vuong, Ted Xiao, Dorsa Sadigh, Chelsea Finn, and Sergey Levine. Octo: An open-source generalist robot policy. In *Proceedings of Robotics: Science and Systems*, Delft, Netherlands, 2024.

- [44] William Peebles, Ilija Radosavovic, Tim Brooks, Alexei A Efros, and Jitendra Malik. Learning to learn with generative models of neural network checkpoints. *arXiv preprint arXiv:2209.12892*, 2022.
- [45] William Peebles and Saining Xie. Scalable diffusion models with transformers. In *Proceedings of the IEEE/CVF international conference on computer vision*, pages 4195–4205, 2023.
- [46] Xue Peng, Erwin Coumans, Tingnan Zhang, Tsang-Wei Lee, Jie Tan, and Sergey Levine. Learning agile robotic locomotion skills by imitating animals. 07 2020.
- [47] Alexander Popov, Alperen Degirmenci, David Wehr, Shashank Hegde, Ryan Oldja, Alexey Kamenev, Bertrand Douillard, David Nistér, Urs Muller, Ruchi Bhargava, et al. Mitigating covariate shift in imitation learning for autonomous vehicles using latent space generative world models. *arXiv preprint arXiv:2409.16663*, 2024.
- [48] Aravind Rajeswaran, Vikash Kumar, Abhishek Gupta, Giulia Vezzani, John Schulman, Emanuel Todorov, and Sergey Levine. Learning Complex Dexterous Manipulation with Deep Reinforcement Learning and Demonstrations. In *Proceedings of Robotics: Science and Systems (RSS)*, 2018.
- [49] Moritz Reuss, Maximilian Li, Xiaogang Jia, and Rudolf Lioutikov. Goal-conditioned imitation learning using score-based diffusion policies. *arXiv preprint arXiv:2304.02532*, 2023.
- [50] Robin Rombach, Andreas Blattmann, Dominik Lorenz, Patrick Esser, and Björn Ommer. High-resolution image synthesis with latent diffusion models. In *Proceedings of the IEEE/CVF conference on computer vision and pattern recognition*, pages 10684–10695, 2022.
- [51] Robin Rombach, Andreas Blattmann, Dominik Lorenz, Patrick Esser, and Björn Ommer. High-resolution image synthesis with latent diffusion models. In *IEEE/CVF Conference on Computer Vision and Pattern Recognition, CVPR 2022, New Orleans, LA, USA, June 18-24, 2022*, pages 10674–10685. IEEE, 2022.
- [52] Mohit Shridhar, Lucas Manuelli, and Dieter Fox. Perceiver-actor: A multi-task transformer for robotic manipulation. In *Proceedings of the 6th Conference on Robot Learning (CoRL)*, 2022.
- [53] Aviv Tamar, Yi Wu, Garrett Thomas, Sergey Levine, and Pieter Abbeel. Value iteration networks. In *Advances in Neural Information Processing Systems*, pages 2154–2162, 2016.
- [54] Wenhui Tan, Bei Liu, Junbo Zhang, Ruihua Song, and Jianlong Fu. Multi-task manipulation policy modeling with visuomotor latent diffusion. *ArXiv*, abs/2403.07312, 2024.
- [55] Julen Urain, Niklas Funk, Jan Peters, and Georgia Chalvatzaki. Se(3)-diffusionfields: Learning smooth cost functions for joint grasp and motion optimization through diffusion. *2023 IEEE International Conference on Robotics and Automation (ICRA)*, pages 5923–5930, 2022.
- [56] Johannes von Oswald, Christian Henning, Benjamin F. Grewe, and João Sacramento. Continual learning with hypernetworks. In *International Conference on Learning Representations*, 2020.
- [57] Kai Wang, Dongwen Tang, Boya Zeng, Yida Yin, Zhaopan Xu, Yukun Zhou, Zelin Zang, Trevor Darrell, Zhuang Liu, and Yang You. Neural network diffusion. *arXiv preprint arXiv:2402.13144*, 2024.
- [58] Manuel Watter, Jost Springenberg, Joschka Boedecker, and Martin Riedmiller. Embed to control: A locally linear latent dynamics model for control from raw images. In *Advances in Neural Information Processing Systems*, pages 2746–2754, 2015.
- [59] Philipp Wu, Alejandro Escontrela, Danijar Hafner, Ken Goldberg, and Pieter Abbeel. Day-dreamer: World models for physical robot learning. *arXiv preprint arXiv:2206.14176*, 2022.
- [60] Zhou Xian and Nikolaos Gkanatsios. Chaineddiffuser: Unifying trajectory diffusion and keypose prediction for robotic manipulation. In *Conference on Robot Learning/Proceedings of Machine Learning Research*. Proceedings of Machine Learning Research, 2023.

- [61] Jiannan Xiang, Guangyi Liu, Yi Gu, Qiyue Gao, Yuting Ning, Yuheng Zha, Zeyu Feng, Tianhua Tao, Shibo Hao, Yemin Shi, Zhengzhong Liu, Eric P. Xing, and Zhiting Hu. Pandora: Towards general world model with natural language actions and video states. 2024.
- [62] Tianhe Yu, Deirdre Quillen, Zhanpeng He, Ryan Julian, Karol Hausman, Chelsea Finn, and Sergey Levine. Meta-world: A benchmark and evaluation for multi-task and meta reinforcement learning. In *Conference on robot learning*, pages 1094–1100. PMLR, 2020.
- [63] Hao Zhang, Zhihan Xu, Jian Liu, and Qingzhao Wang. Generalized and efficient planning with scalable latent world models. *arXiv preprint arXiv:2406.10667*, 2024.
- [64] Weidong Zhang, Jian Liu, Lihe Xia, Qingzhao Wang, and Hongming Zhou. Safedreamer: Safe reinforcement learning with world models. *arXiv preprint arXiv:2307.07176*, 2023.
- [65] Ruijie Zheng, Ching-An Cheng, Hal Daumé Iii, Furong Huang, and Andrey Kolobov. Prise: Llm-style sequence compression for learning temporal action abstractions in control. In *International Conference on Machine Learning*, pages 61267–61286. PMLR, 2024.
- [66] Gaoyue Zhou, Hengkai Pan, Yann LeCun, and Lerrel Pinto. Dino-wm: World models on pre-trained visual features enable zero-shot planning. *arXiv preprint arXiv:2411.04983*, 2024.

## A Appendix

### A.1 VAE loss derivation

Since  $a_t \sim \mathcal{N}(\pi(s_t, \theta), \sigma^2)$ :

$$p(a_t | s_t, \theta) = \frac{1}{\sqrt{2\pi\sigma^2}} \exp\left(-\frac{(a_t - \pi(s_t, \theta))^2}{2\sigma^2}\right) \quad (6)$$

Our objective is to maximize the *mELBO*. The negative log likelihood of trajectory  $\tau_k = \{s_t^k, a_t^k\}_{t=1}^T$  for the given VAE parameters is:

$$\begin{aligned} \mathcal{L}(\tau_k | \phi_{enc}, \phi_{dec}, \phi_{wm}) &= -\sum_{t=1}^T \mathbb{E}_{q_{\phi_{enc}}(z|\tau_k)} \left[ \mathbb{E}_{p_{\phi_{dec}}(\theta|z)} \left[ \log p(a_t^k | s_t^k, \theta) \right] \right] \\ &\quad - \sum_{t=2}^T \mathbb{E}_{q_{\phi_{enc}}(z|\tau_k)} \left[ \mathbb{E}_{p_{\phi_{dec}}(\theta|z)} \left[ \log p_{\phi_{wm}}(s_t^k | s_{t-1}^k, a_{t-1}^k) \right] \right] \\ &\quad + \text{KL}(q_{\phi_{enc}}(z | \tau_k) \| p(z)) \end{aligned} \quad (7)$$

Consider the second term in the above equation. On maximization  $a_{t-1}^k = \pi(s_{t-1}^k, \theta)$ , and because the inner quantity is a constant w.r.t.  $s_t$  we can add a harmless expectation  $\mathbb{E}_{s_t \sim \pi[\cdot]}$  (i.e., states visited by the estimated policy, not necessarily those in the dataset), therefore it becomes:

$$\begin{aligned} &\mathbb{E}_{q_{\phi_{enc}}(z|\tau_k)} \left[ \mathbb{E}_{p_{\phi_{dec}}(\theta|z)} \left[ \mathbb{E}_{s_t \sim \pi} \left[ \log p_{\phi_{wm}}(s_t^k | s_{t-1}^k, \pi(s_{t-1}^k, \theta)) \right] \right] \right] \\ &= \mathbb{E}_{q_{\phi_{enc}}(z|\tau_k)} \left[ \mathbb{E}_{p_{\phi_{dec}}(\theta|z)} \left[ \mathbb{E}_{s_t \sim \pi} \left[ \log \frac{p_{\phi_{wm}}(s_t^k | s_{t-1}^k, \pi(s_{t-1}^k, \theta))}{p_{\phi_{wm}}(s_t^k | s_{t-1}^k, a_{t-1}^k)} \right] \right] \right] \\ &\quad + \mathbb{E}_{q_{\phi_{enc}}(z|\tau_k)} \left[ \mathbb{E}_{p_{\phi_{dec}}(\theta|z)} \left[ \mathbb{E}_{s_t \sim \pi} \left[ \log p_{\phi_{wm}}(s_t^k | s_{t-1}^k, a_{t-1}^k) \right] \right] \right] \end{aligned} \quad (8)$$

We can now substitute in the KL term, and drop the expectation in the last term (since the inner terms only depend on  $s_{t-1}^k$  and not  $s_t \sim \pi, \theta$ , or  $z$ ). Therefore, the loss now becomes:

$$\begin{aligned} \mathcal{L}(\tau_k | \phi_{enc}, \phi_{dec}, \phi_{wm}) &= C + \frac{1}{2\sigma^2} \sum_{t=1}^T \mathbb{E}_{q_{\phi_{enc}}(z|\tau_k)} \left[ \mathbb{E}_{p_{\phi_{dec}}(\theta|z)} \left[ (a_t^k - \pi(s_t^k, \theta))^2 \right] \right] \\ &\quad + \sum_{t=2}^T \mathbb{E}_{q_{\phi_{enc}}(z|\tau_k)} \left[ \mathbb{E}_{p_{\phi_{dec}}(\theta|z)} \left[ \text{KL}(p_{\phi_{wm}}(s_t^k | s_{t-1}^k, \pi(s_{t-1}^k, \theta)) \| p_{\phi_{wm}}(s_t^k | s_{t-1}^k, a_{t-1}^k)) \right] \right] \\ &\quad - \sum_{t=2}^T \log p_{\phi_{wm}}(s_t^k | s_{t-1}^k, a_{t-1}^k) \\ &\quad + \text{KL}(q_{\phi_{enc}}(z | \tau_k) \| p(z)) \end{aligned} \quad (9)$$

For computational stability, we construct our decoder to be a deterministic function  $f_{\phi_{dec}}$ , i.e.,  $p_{\phi_{dec}}(\theta | z)$  becomes  $\delta(\theta - f_{\phi_{dec}}(z))$ . Further, if we have a trained world model, we can approximate  $s_t^k$  with  $s_t$  (i.e., direct model output samples) in the second term. This is done so that we can optimize the world model and policy correction separately with the teacher forcing and rollout objectives

(similar to that followed in [1]. Therefore:

$$\begin{aligned}
& \mathcal{L}(\tau_k | \phi_{enc}, \phi_{dec}, \phi_{wm}) \\
&= C + \frac{1}{2\sigma^2} \sum_{t=1}^T \mathbb{E}_{q_{\phi_{enc}}(z|\tau_k)} [(a_t^k - \pi(s_t^k, f_{\phi_{dec}}(z)))^2] \\
&+ \sum_{t=2}^T \mathbb{E}_{q_{\phi_{enc}}(z|\tau_k)} [\text{KL}(p_{\phi_{wm}}(s_t | s_{t-1}^k, \pi(s_{t-1}^k, f_{\phi_{dec}}(z))) \| p_{\phi_{wm}}(s_t | s_{t-1}^k, a_{t-1}^k))] \\
&- \sum_{t=2}^T \log p_{\phi_{wm}}(s_t^k | s_{t-1}^k, a_{t-1}^k) \\
&+ \text{KL}(q_{\phi_{enc}}(z | \tau_k) \| p(z))
\end{aligned}$$

Where  $C$  is a constant from the substitution. Enforcing  $p(z) = \mathcal{N}(0, I)$ , and ignoring constants, we get:

$$\mathcal{L}(\tau_k | \phi_{enc}, \phi_{dec}, \phi_{wm}) = \mathcal{L}_{BC} + \mathcal{L}_{RO} + \mathcal{L}_{TF} + \mathcal{L}_{KL} \quad (10)$$

$$\mathcal{L}_{BC} = \sum_{t=1}^T \mathbb{E}_{q_{\phi_{enc}}(z|\tau_k)} [(a_t^k - \pi(s_t^k, f_{\phi_{dec}}(z)))^2] \quad (11)$$

$$\mathcal{L}_{RO} = \sum_{t=2}^T \mathbb{E}_{q_{\phi_{enc}}(z|\tau_k)} [\text{KL}(p_{\phi_{wm}}(s_t | s_{t-1}^k, \pi(s_{t-1}^k, f_{\phi_{dec}}(z))) \| p_{\phi_{wm}}(s_t | s_{t-1}^k, a_{t-1}^k))] \quad (12)$$

$$\mathcal{L}_{TF} = \sum_{t=2}^T (s_t^k - \hat{s}_t^k)^2 \quad (13)$$

$$\mathcal{L}_{KL} = \beta_{kl} \sum_{i=1}^{\dim(z)} (\sigma_{e_i}^2 + \mu_{e_i}^2 - 1 - \log \sigma_{e_i}^2) \quad (14)$$

where,  $\mathcal{L}_{BC}$  is the behavior cloning loss to train the policy decoder,  $\mathcal{L}_{RO}$  is the rollout loss to correct the decoded policy's actions using the world model,  $\mathcal{L}_{TF}$  is the teacher forcing loss to train the world model,  $\mathcal{L}_{KL}$  is the KL loss to regularize the latent space,  $(\mu_e, \sigma_e) = f_{\phi_{enc}}(\tau_k)$ ,  $z \sim \mathcal{N}(\mu_e, \sigma_e)$ ,  $\hat{s}_t^k \sim p_{\phi_{wm}}(s_t^k | s_{t-1}^k, a_{t-1}^k)$  and  $\beta_{kl}$  is the regularization weight.

## A.2 Ablations

### A.3 Diffusion Model Architecture

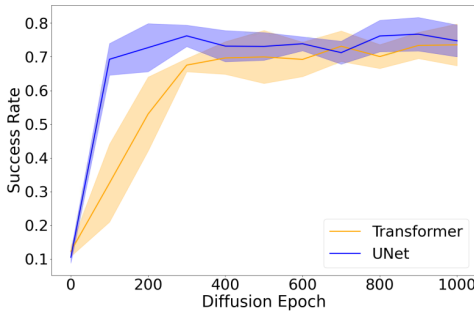


Figure 8: Diffusion Architecture Ablation

Diffusion models typically adopt either UNet-based [27] or Transformer-based [45] architectures (described as medium "m" in Section A.8.1). To guide our choice for the WARPd diffusion policy, we performed an ablation study on the PushT task [10] using an action horizon of 32. As shown in Figure 8, the UNet model demonstrated faster initial learning, achieving higher average success rates early in training. However, both architectures eventually converged to comparable final success rates. For consistency, we adopt the UNet architecture for all other experiments.

### A.4 Decoder size

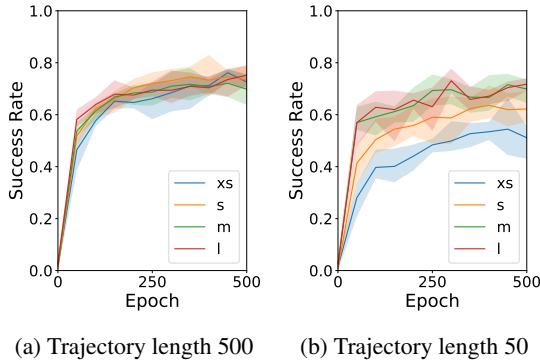


Figure 9: **Effect of VAE decoder size:** For long trajectories, even the smallest decoder (*xs*) yields high task performance, whereas short trajectories benefit from a larger decoder.

that despite the substantial parameter count of the hypernetwork decoder, the resulting inferred policy remains relatively small ( $< 100K$  parameters, see Figure 6). The results demonstrate that increasing the decoder size consistently improves the average success rate of the decoded policies. Refer Section A.8.3 for more details regarding the decoder size characterization.

This contrasts with rollouts from the HalfCheetah environment, where even smaller decoders generated accurate policies from trajectory snippets. We hypothesize this discrepancy stems from two key factors. First, the cyclic nature of HalfCheetah provides sufficient information within snippets to infer the underlying policy. Second, the increased complexity of Metaworld tasks means that snippets may lack crucial information for inference. For instance, in a pick-and-place task, a snippet might only capture the "pick" action, leaving the latent without sufficient information to infer the "place" action.

#### A.4.1 KL coefficient

A key hyperparameter in WARPd is the KL regularization term,  $\beta_{KL}$ , used during VAE training. In this section, we analyze its impact on the learned latent space using the PushT task with an action horizon of 32. We train three VAEs with  $\beta_{KL}$  values of  $1e-7$ ,  $1e-9$ , and  $1e-10$ . For evaluation, we sample a trajectory of length 32, encode and decode it via the VAE to generate a policy, and then execute this policy in the environment starting from the same initial state. We compute the MSE between the final state reached after 32 steps and the corresponding state in the original trajectory. Figure 10 in Figure 11 shows this metric across 3 seeds during training. Lower  $\beta_{KL}$  values result in lower final-state MSE, indicating better trajectory reconstruction. This is due to a more expressive,

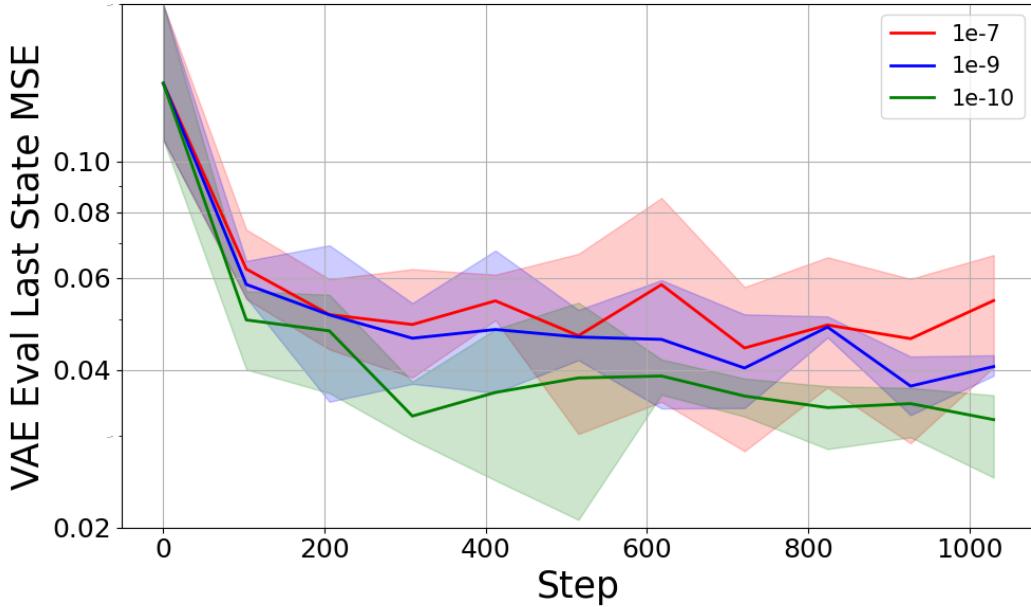


Figure 10: **Effect of KL coefficient**

multi-modal latent space made possible by weaker regularization, without compromising sampling, as diffusion still operates effectively within this space. Visualizations are provided below in Figure 11. Based on these results, we use  $\beta_{\text{KL}} = 1\text{e-}10$  in all PushT experiments.

Following the KL ablation experiment above, we analyzed the latent space of the encoded trajectories with PCA, similar to that performed in Section A.6. The three plots in Figure 11, show that the trajectory encodings get closer and lose behavioral diversity when the KL coefficient is high.

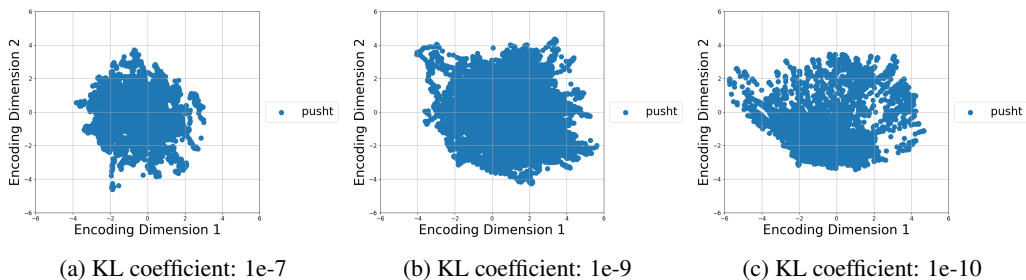


Figure 11: Latent space representation of PushT trajectories at different KL coefficients

## A.5 Metaworld task descriptions

## A.6 Effect of Trajectory snipping on Latent Representations

For most robotics use cases, it is impossible to train on long trajectories due to the computational limitations of working with large batches of long trajectories. In some cases, it may also be beneficial to generate locally optimum policies for shorter action horizons (as done for experiments presented in Section 4.1.1). Therefore, we analyze the effect of sampling smaller sections of trajectories from the dataset. After training a VAE for the D4RL half-cheetah dataset on three policies (expert, medium, and random), we encode all the trajectories in the mixed dataset to the latent space. We then perform Principal Component Analysis (PCA) on this set of latents and select the first two principal components. Figure 12a shows us a visualization of this latent space. We see that the VAE has learned to encode the three sets of trajectories to be well separable. Next, we run the same experiment, but now we sample trajectory snippets of length 100 from the dataset instead of the full-length (1000) trajectories. Figure 12b shows us the PCA on the encoded latents of these trajectory snippets. We see

Task	Description
Window Open	Push and open a window. Randomize window positions
Door Open	Open a door with a revolving joint. Randomize door positions
Drawer Open	Open a drawer. Randomize drawer positions
Dial Turn	Rotate a dial 180 degrees. Randomize dial positions
Faucet Close	Rotate the faucet clockwise. Randomize faucet positions
Button Press	Press a button. Randomize button positions
Door Unlock	Unlock the door by rotating the lock clockwise. Randomize door positions
Handle Press	Press a handle down. Randomize the handle positions
Plate Slide	Slide a plate into a cabinet. Randomize the plate and cabinet positions
Reach	Reach a goal position. Randomize the goal positions

Table 2: Metaworld task descriptions and randomization settings

that the separability is now harder in the latent space. Surprisingly, we noticed that after training our VAE on the snippets, the decoded policies from randomly snipped trajectories were still faithfully behaving like their original policies. We believe that this is because the halfcheetah env is a cyclic locomotion task, and all trajectory snippets have enough information to indicate its source policy. More dimensions of the PCA are shown in Figure 13.

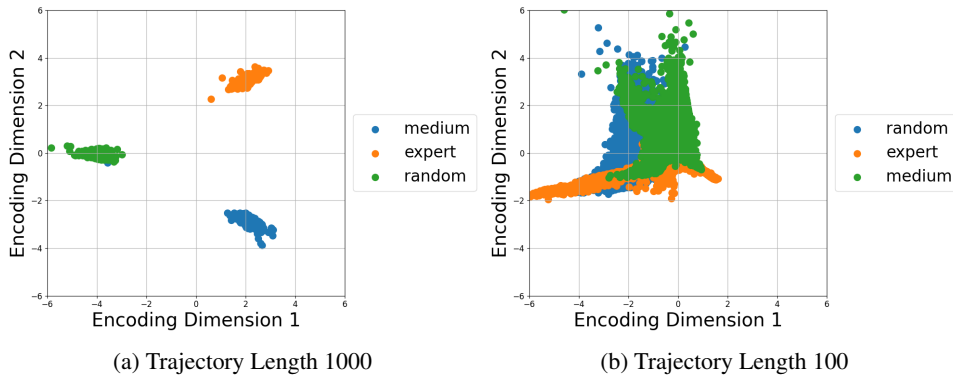


Figure 12: **Effect of trajectory snipping** in HalfCheetah. Top two principal components of the latent.

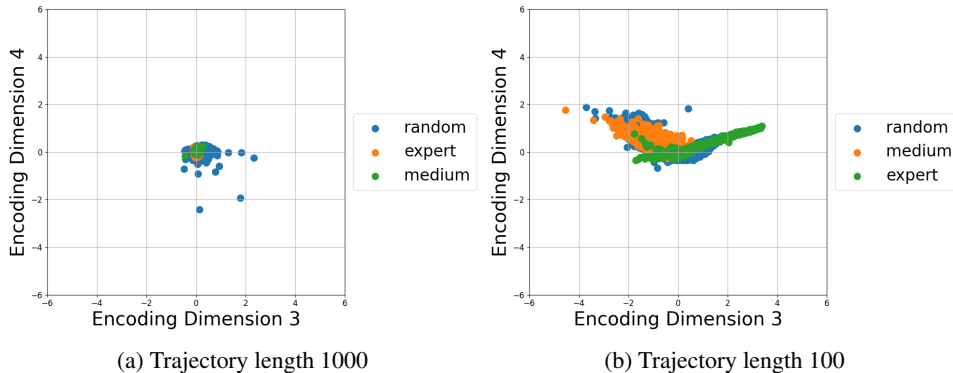


Figure 13: **Effect of trajectory snipping** in HalfCheetah. Top third and fourth principal components of the latent.

To validate this hypothesis, we analyze our method on trajectory snippets for non-cyclic tasks. We choose the MT10 suite of tasks in Metaworld [62] (note that these are different from the original 10 tasks discussed in the rest of the paper). We utilize the hand-crafted expert policy for each of the tasks in MT10 to collect trajectory data. For each task, we collect 1000 trajectories of length 500.

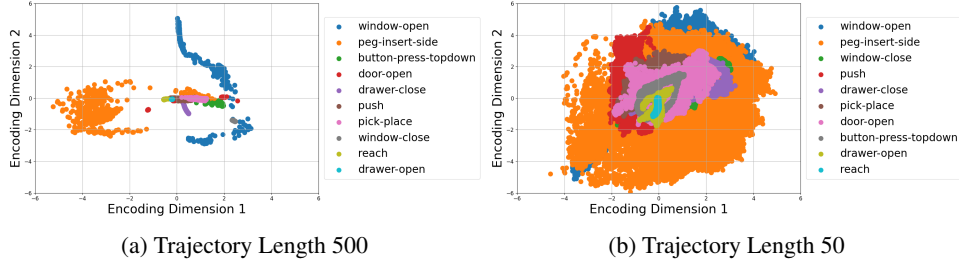


Figure 14: **Effect of trajectory snipping** in MT10. Top two principal components of the latent.

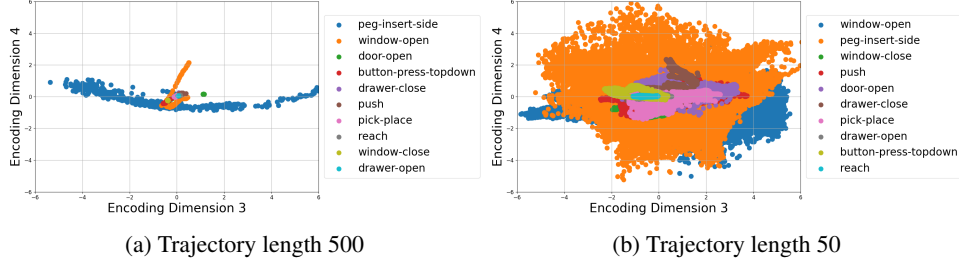


Figure 15: **Effect of trajectory snipping** in MT10. Top third and fourth principal components of the latent.

Figure 14a shows the principal components of the latents of the full trajectories in the dataset, and Figure 14b shows the same for the split trajectories. We can see that the separability of different tasks is much harder in this case. More dimensions of the PCA are shown in Figure 15b. Further, we noticed that the decoded policies from the trajectory snippets did not perform as well as the original policies - for the same decoder size as the half cheetah task. This validates our hypothesis that the snippets are unable to reproduce the original policy for non-cyclic tasks. To have the same degree of behavior reconstruction as the half-cheetah tasks, we need a larger decoder model. This is discussed in Section A.4.

## A.7 Behavior Reconstruction Analysis

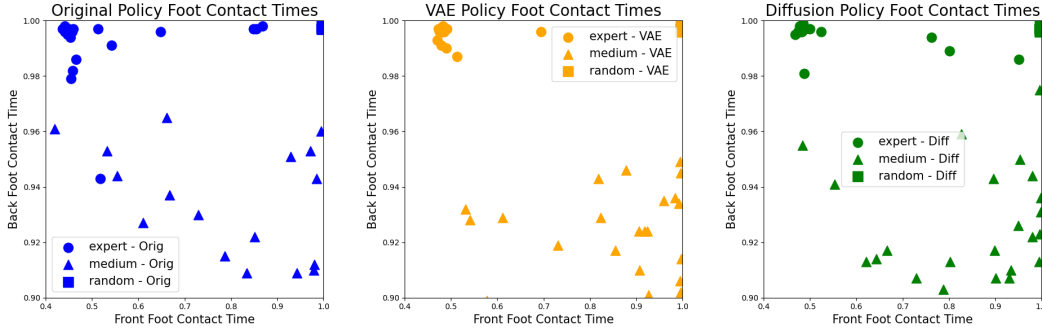
Here, we ask – Does WARPD reconstruct the original policies and reproduce diverse behaviors?

### A.7.1 Locomotion

First, we analyze the behavior reconstruction capability of different components of WARPD in locomotion domains. For this experiment, we use the halfcheetah dataset from D4RL [15]. The parameters used for this experiment are shown in Section A.8.5. Each trajectory in this dataset has a length of 1000. We combine trajectory data from three original behavior policies provided in this dataset: expert, medium, and random. Following [3], we track the foot contact timings of each trajectory as a metric for measuring behavior. For each behavior policy, we get 32 trajectories. These timings are normalized to the trajectory length and are shown in Figure 16. For each plot, the x-axis denotes the foot contact percentage of the front foot, while the y-axis denotes the foot contact percentage of the back foot.

We first visualize the foot contact timings of the original policies in Figure 16a. We see that different running behaviors of the half cheetah can be differentiated in this plot. Then, we train the VAE model on this dataset to embed our trajectories into a latent space. We then apply the hypernetwork decoder to generate policies from these latents. These policies are then executed on the halfcheetah environment, to create trajectories. We plot the foot contact timings of these generated policies in Figure 16b. We see that the VAE captures each of the original policy’s foot contact distributions, therefore empirically showing that the assumption  $p_{\phi_{dec}}(\theta | z) = \delta(\theta - f_{\phi_{dec}}(z))$  is reasonable. Then, we train a latent diffusion model conditioned on a behavior specifier (i.e., one task ID per behavior). In Figure 16c, we show the distribution of foot contact percentages of the policies generated by

the behavior specifier conditioned diffusion model. We see that the diffusion model can learn the conditional latent distribution well, and the behavior distribution of the decoded policies of the sampled latent matches the original distribution. Apart from visual inspection, we also track rewards obtained by the generated policies and empirically calculated Jensen Shannon Divergence between the original and obtained foot contact distributions and observe that WARPDP maintains behavioral diversity in this locomotion task. See below for more details.



(a) Original policies that provide the trajectory dataset. (b) VAE generated policies from trajectories. (c) Diffusion generated policies from trajectories.

**Figure 16: Foot-contact times shown for various trajectories on the Half Cheetah task.** We use foot contact times as the chosen metric to show different behaviors for the half cheetah run task by different policies. The first plot on the left shows the distribution of foot contact percentages for each of the three original policies. The second plot in the center denotes the foot contact percentages for the policies generated by the trained VAE when provided each original policy’s entire trajectory. The third plot on the right denotes the foot contact percentages for the policies generated by the diffusion model, trained without any task conditioning.

We can analyze the behavior reconstruction capability of WARPDP by comparing the rewards obtained during a rollout. The VAE parameters used for this experiment are shown in Section A.8.5. Figure 17 shows us the total objective obtained by the original, VAE-decoded, and diffusion-denoised policies. We see that the VAE-decoded and diffusion-generated policies achieve similar rewards to the original policy for each behavior.

Apart from these plots, we use Jensen-Shannon divergence to quantify the difference between two distributions of foot contact timings. Table 3 shows the JS divergence between the empirical distribution of the foot contact timings of the original policies and those generated by WARPDP. The lower this value is, the better. As a metric to capture the stochasticity in the policy and environment, we get the JS divergence between two successive sets of trajectories generated by the same original policy, which we shall denote SOS (Same as source). A policy having a JS divergence score lesser than this value indicates that that policy is indistinguishable from the original policy by behavior. As a baseline for this experiment, we train a large (5-layer, 512 neurons each) behavior-conditioned MLP on the same mixed dataset with MSE loss. We see that policies generated by WARPDP consistently achieve a lower JS divergence score than the MLP baseline for expert and medium behaviors. The random behavior is difficult to capture as the actions are almost Gaussian noise. Surprisingly, for the HalfCheetah environment, policies generated by WARPDP for expert and medium had lower scores than SOS, making it behaviorally indistinguishable from the original policy.

### A.7.2 Manipulation

To verify the behavior reconstruction capabilities of WARPDP in manipulation, we also experiment on the D4RL Adroit dataset [48]. We choose a tool use task, where the agent must hammer a nail into a board. We utilize their 5000 expert and 5000 human-cloned trajectories, to train our WARPDP model. The implementation details are in Section A.8.6. Then, we evaluate the behavior of the original and generated policy on the following metrics: **Mean object height** - Average height of the object during eval; **Alignment error (goal distance)** - Mean distance between the target and the final goal position; **Max nail impact** - Maximum value of the nail impact sensor during eval; **Contact ratio** - Fraction of time steps where the nail impact sensor value exceeds 0.8; **Object manipulation score** - Proportion

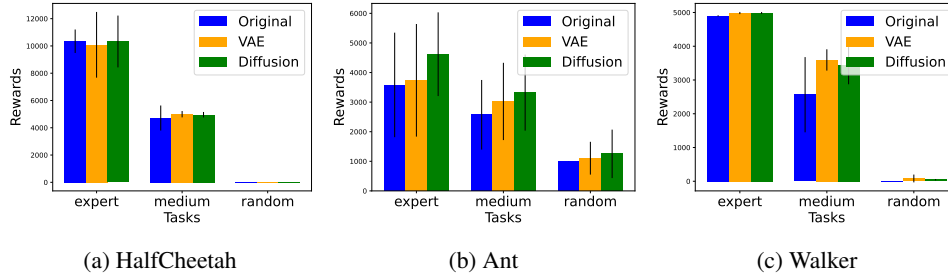


Figure 17: **Reconstruction Rewards:** For each of the 3 environments shown above, the generated policy from trajectory decoded VAE and task-conditioned diffusion model, achieves similar total objective as the original policies. Each bar indicates the mean total objective obtained with error lines denoting the standard deviation.

Environment	Source Policy	Target Policy		
		SOS	MLP	WARPD
Ant	Expert	$0.187 \pm 0.142$	$1.272 \pm 0.911$	$0.510 \pm 0.159$
	Medium	$0.624 \pm 0.232$	$1.907 \pm 0.202$	$1.328 \pm 0.283$
	Random	$1.277 \pm 1.708$	$4.790 \pm 0.964$	$8.859 \pm 0.792$
HalfCheetah	Expert	$0.158 \pm 0.146$	$2.810 \pm 1.139$	$0.088 \pm 0.050$
	Medium	$0.275 \pm 0.196$	$0.692 \pm 0.787$	$0.194 \pm 0.157$
	Random	$0.0467 \pm 0.009$	$0.11 \pm 0.009$	$0.104 \pm 0.0187$
Walker2D	Expert	$0.342 \pm 0.329$	$2.879 \pm 1.493$	$1.093 \pm 0.310$
	Medium	$0.078 \pm 0.058$	$0.165 \pm 0.126$	$0.155 \pm 0.091$
	Random	$0.080 \pm 0.004$	$60.514 \pm 52.461$	$2.776 \pm 1.260$

Table 3: **Behavior Reconstruction:** JS divergence between foot contact distributions from source and target policies. The lower the value, the better.

of time steps where the object height exceeds 0.04 meters. From Figure 18, we can see that the policy generated by WARPD behaves similarly to the original policy.

## A.8 Implementation Details

The following are the hyperparameters we use for our experiments:

### A.8.1 Baseline Diffusion Policy model

To train the diffusion policy baseline model shown in Figure 6, we utilize the training script provided by the authors of DP here:

<https://colab.research.google.com/drive/1gxdkgRVfM55zihY9TFLja97cSVZOZq2B?usp=sharing>.

To set the model size we use the following parameters:

Size	Diffusion Step Embed Dim	Down Dims	Kernel Size
extra-small: (s)	64	[16, 32, 64]	5
small: (s)	256	[32, 64, 128]	5
large: (m)	256	[128, 256, 256]	5
large: (l)	256	[256, 512, 1024]	5
extra large: (xl)	512	[512, 1024, 2048]	5

Table 4: Architectural configurations for the ConditionUnet1D Diffusion Policy (DP) across different model sizes.

For the ablation described in Section A.3, we use a transformer architecture, the details of which are:

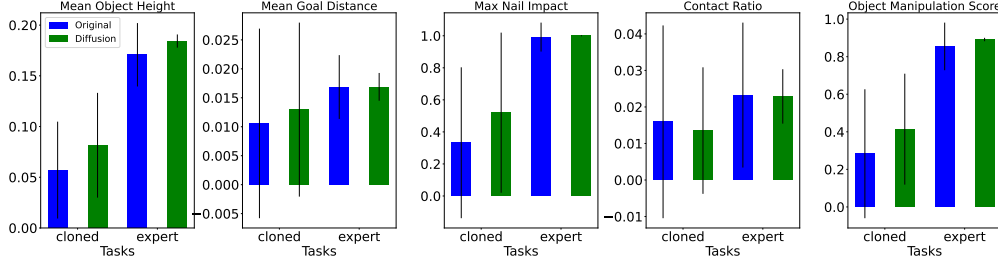


Figure 18: **Behavior Reconstruction for Manipulation:** We track these metrics on the Adroit hammer task, and the WARPED-generated policy behaves similarly to the original policy. The ‘cloned’ bars represent metrics with respect to a human demonstration behavior cloned policy, and ‘expert’ bars represent metrics from an RL-trained policy.

Size	Diffusion Step Embed Dim	Model Dim	# Layers	# Heads
extra-small: (xs)	64	64	3	2
small: (s)	128	128	4	4
medium: (m)	256	256	6	8
large: (l)	256	512	8	8
extra-large: (xl)	512	768	12	12

Table 5: Architectural configurations for Transformer-based Diffusion models across different model sizes.

### A.8.2 VAE Encoder details

For the encoder, we first flatten the trajectory to form a one-dimensional array, which is then fed to a Multi-Layer Perceptron with three hidden layers of 512 neurons each.

### A.8.3 VAE Hypernetwork decoder size characterization

For the hypernetwork, we utilize an HMLP model (a full hypernetwork) from the <https://hypnettorch.readthedocs.io/en/latest/> package with default parameters. We condition the HMLP model on the generated latent of dimension 256. To vary the size of the decoder, as explained in Section A.4, we set the hyperparameter in the HMLP as shown in Table 6

Size	No. of parameters	layers
xs	3.9M	[50, 50]
s	7.8M	[100, 100]
m	15.6 M	[200, 200]
l	31.2M	[400, 400]

Table 6: VAE size varying parameters

### A.8.4 Diffusion model parameters

For all our experiments, we utilize the same ConditionalUnet1D network from [10] as the diffusion model. This is the same as the DP-medium (m) model described in Section A.8.1.

### A.8.5 Mujoco locomotion tasks

We use the following hyperparameters to train VAEs for all D4RL mujoco tasks shown in the paper. To show the effect of shorter trajectories in Section A.6, we change the Trajectory Length to 100.

### A.8.6 Adroit Hammer task

We use the same hyperparameters as Table 7 and override the following hyperparameters to train VAEs for the D4RL Adroit hammer task shown in the paper.

Parameter	Value
Trajectory Length	1000
Batch Size	32
VAE Num Epochs	150
VAE Latent Dimension	256
VAE Decoder Size	s
Evaluation MLP Layers	{256, 256}
VAE Learning Rate	$3 \times 10^{-4}$
KL Coefficient	$1 \times 10^{-6}$
Diffusion Num Epochs	200

Table 7: Mujoco locomotion hyperparameters.

Parameter	Value
Trajectory Length	128
VAE Num Epochs	20
Diffusion Num Epochs	10

Table 8: Adroit hammer hyperparameters.

Further, for the experiment where we show the hammer task can be composed of sub-tasks, we change the Trajectory Length to 32 to enable WARPDP to learn the distribution of shorter horizon policies.

#### A.8.7 PushT and Robomimic WARPDP

For all the experiments shown in Section 4.1.1, we use the same hyper-parameters described in Table 7, and override the following:

Parameter	Value
Trajectory Length	256
VAE Num Epochs	1000
Diffusion Num Epochs	1000
Diffusion Model size	1
VAE Decoder Size	1
VAE KL coefficient	$1e - 10$

Table 9: PushT WARPDP hyperparameters.

#### A.8.8 Metaworld tasks

For all the experiments shown in Section 4.1.2, we use the same hyper-parameters described in Table 7, and override the following:

Parameter	Value
Trajectory Length	500
VAE Num Epochs	100
Diffusion Num Epochs	100
VAE Decoder Size	xs

Table 10: Metaworld hyperparameters.

To show the effect of shorter trajectories in Section A.6, we change the Trajectory Length to 50.

### A.9 Compute Resources

Each VAE and diffusion experiment was run on jobs that were allocated 6 cores of a Intel(R) Xeon(R) Gold 6154 3.00GHz CPU, an NVIDIA GeForce RTX 2080 Ti GPU, and 108 GB of RAM.

Our observations indicate that the training time for each component of WARP is approximately equivalent to that of a full DP training run:  $\text{traintime}(\text{DP}) \simeq \text{traintime}(\text{VAE}_{\text{WARP}}) \simeq \text{traintime}(\text{Diffusion}_{\text{WARP}})$

Therefore, the total training time for WARP is approximately  $2 * \text{traintime}(\text{DP})$ . To provide a concrete example, for the PushT task with image observations, using a compute configuration of a Tesla P100-PCIE-16GB GPU, 16 Intel Xeon Gold 6130 CPU cores, and 64GB RAM, we observed the following wall-clock training times:

- 2000 epochs of DP training: 13 hours 8 minutes
- 1000 epochs of WARP's VAE training: 12 hours 32 minutes
- 1000 epochs of WARP's diffusion training: 13 hours 37 minutes